First demonstration of a sub-keV electron recoil energy threshold in a liquid argon ionization chamber

S. Sangiorgio,[1, *] A. Bernstein,[1] J. Coleman,[2] M. Foxe,[3] C. Hagmann,[1] T. H. Joshi,[1, 4]
I. Jovanovic,[3] K. Kazkaz,[1] K. Mavrokoridis,[2] V. Mozin,[1] S. Pereverzev,[1] and P. Sorensen[1]

[1]*Lawrence Livermore National Laboratory, 7000 East Ave., Livermore, CA 94550, USA*
[2]*Department of Physics, University of Liverpool, Oxford St, Liverpool, L69 7Ze, UK*
[3]*Dept. of Mechanical and Nuclear Engineering, Pennsylvania State University, University Park, PA 16802*
[4]*Department of Nuclear Engineering, University of California, Berkeley, CA 94720, USA*

We make a first demonstration of a sub-keV electron recoil energy threshold in a dual-phase liquid argon time-projection chamber. This is an important step in a program to build a detector capable of identifying the ionization signal resulting from nuclear recoils at a few keV and below. We obtained this result by observing the peaks in the energy spectrum at 2.82 keV and 0.27 keV, following the K- and L-shell electron capture decay of ^{37}Ar. We describe the details of the ^{37}Ar source preparation, as this calibration technique may prove useful, e.g. for dark matter direct detection experiments. A ^{55}Fe internal x-ray source was also measured simultaneously and provided another calibration point at 5.9 keV. We discuss the ionization yield and electron recombination in liquid argon at the three calibration energies.

I. INTRODUCTION

Dual-phase noble liquids detectors have become a popular choice for WIMP dark matter experiments thanks to their target mass scalability, low background, and low threshold. More recently, they have been proposed also to search for coherent neutrino-nucleus scattering (CNNS). In both cases, the only signature in the detector is a low- energy nuclear recoil. For the most common WIMP scenarios, nuclear recoil energies between 10-100 keVr in liquid Ar or Xe are expected [1]. For CNNS, detection sensitivity to nuclear recoils of a few hundred eVr is needed, especially if reactor neutrinos are employed [2]. Energy thresholds of 5-10 keVr are commonly obtained in dark matter experiments with liquid xenon or argon. The XENON10 experiment recently showed that an energy threshold as low as 1 keVr, corresponding to only a handful of ionized electrons, might be obtained [3] in liquid xenon. This result was obtained from extrapolation of the model described in [4]. It is essential to measure the low-energy response of noble gas detectors to allow their use for CNNS, and to probe broader ranges of light-mass WIMPs.

Here we report the first demonstration of sub-keV electron-recoil spectroscopy in a dual-phase argon detector. This is achieved by detecting the proportional scintillation produced in the gas phase by ionization electrons after they have been extracted from the liquid. Specifically, we observed the 270 eV cascade following L-shell electron capture in ^{37}Ar. We use the single electron signal as an absolute calibration for the ionization channel. We then suggest that low energy electron recoils can be modeled within an existing framework. The results shown here are a first step toward providing detector capability to measure the ionization yield of nuclear recoils at few keVr and below, as well as for enhancing the reach of axion search via the axio-electric effect.

In liquified noble gas detectors, the energy transferred to the medium by a particle results results in ionization, scintillation and heat [5]. The fraction lost to each channel depends on both the incident particle type and energy. Indeed electron recombinations varies with ionization density along the track as well as the electric field. A discussion of the mechanism and yields of energy transfer in liquefied noble gases lies outside the scope of this paper. Extensive literature is available on the subject (see for example [6] and references therein). However data are still scarce at low energies for both electron and nuclear recoils. In addition, the measurements have mostly focused so far on scintillation yields alone, rather than ionization.

II. DETECTOR AND CALIBRATION SOURCES

We have built a prototype dual-phase liquid argon time-projection chamber in the context of our program to detect coherent neutrino-nucleus scattering [7]. Our detector emphasizes high-sensitivity measurement of the ionization signal by means of secondary scintillation in the gas region. A particle interaction in the liquid phase produces primary scintillation (S1) and ionization [5]. The electrons are drifted away from the interaction site by an electric field and extracted into the gas where they create secondary scintillation (S2) that we detect. light collection was optimized for the S2 rather than S1 signal, and as a result limits the detection of S1 below about 10 keV.

A schematic view of the detector is provided in Fig. 1. It consists of ∼100 g of liquid argon as the active volume surrounded on the bottom and sides by ∼1 kg of inactive liquid. A gaseous region extends on top of the liquid and is kept at a constant pressure of ∼820 torr.
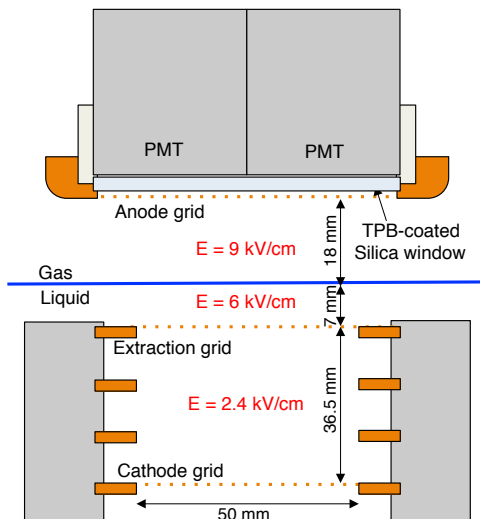
FIG. 1. Schematic drawing of the vertical cross section of the detector central region. The four copper rings are negatively biased and shape the electric field in the drift region. The anode is at ground potential. A SS mesh (50 mesh/inch, 30 μm dia wire, 88% optical transparency) is used for the anode and cathode grids. The extraction grid is obtained using 15 μm SS wire with 1 mm spacing. The scintillation light is collected by four 1" PMTs through a TPB-coated silica window. The electric fields used to obtain the data reported here are also shown.

The temperature of the gas is that of the Ar vapor at that pressure. The active volume is 3.65 cm high, and 5 cm in diameter. A set of four copper rings delimits this active volume and shapes the electric field needed to drift the electrons in the liquid. An extraction grid is placed 5-10 mm below the liquid level, while the anode is located 2.5 cm above the extraction grid. Electric fields up to 4 kV/cm in the drift region and up to 10 kV/cm in the gain were achieved. The argon scintillation light is detected through a fused silica window by a squared array of four 1" Hamamatsu R8520 photomultiplier tube (PMT) modified for cryogenic operation. A 0.05 mg/cm^2 coating of TetraPhenyl Butadiene (TPB) over the silica window acts as wavelength shifter for the Ar UV scintillation light [8]. The PMTs signals are triggered and digitized at 500 MHz using a LeCroy Waverunner 104MXi-A 8 bit digital oscilloscope.

The detector response was studied using different gamma sources. A 500μCi ^{241}Am gamma source was collimated to produce a thin ($\sim$2 mm) beam spanning the entire drift region of the detector. Photoelectric events (60 keV) from the ^{241}Am were used to assess argon purity by measuring the electron lifetime extracted from the dependance of the total ionization signal from event depth in the liquid. The latter is calculated using the time delay between the S1 and S2 scintillation signals. For the measurements reported here, no appreciable loss of electrons due to impurities was observed within the detector's energy resolution for events produced at dif-

ferent depths. The ^{241}Am purity data were taken at a drift field of 3.0 kV/cm.

Two sources located within the active liquid volume were used for calibration of the detector to low energy electron recoils. A 5 mm diameter electroplated ^{55}Fe bare source provided 5.90 keV and 6.49 keV x-rays with $\sim$ 1 kBq activity. The source was mounted on a movable arm located just above the cathode inside the liquid argon active volume.

In addition, for the first time in a dual-phase detector, we used ^{37}Ar as a diffused source throughout the active region. ^{37}Ar was obtained from neutron irradiation of ^{nat}Ar at McClellan Nuclear Research Center, similarly to what described in [9]. ^{nat}Ar is composed by ^{40}Ar (99.6%), ^{36}Ar (0.34%) and ^{38}Ar (0.06%). The irradiation therefore produces mainly ^{41}Ar that quickly decays with a half-life of 110 minutes, leaving ^{37}Ar as the only significant radioactive product. ^{37}Ar decays by electron capture (EC) to the ground state of ^{37}Cl with a half life of 35 days. The atomic shell cascade processes result in a total energy release of 2.82 keV for capture on the K-shell and 0.27 keV for capture on the L-shell [10]. For our production, 1 liter of ^{nat}Ar at 11 bar was placed next to the reactor core and irradiated for 4 hours to produce 30 μCi of ^{37}Ar. The activity was verified by measuring gamma emission from ^{41}Ar shortly after irradiation. The gas was then cryogenically extracted, transferred to a lecturer's cylinder and pressurized with ^{nat}Ar to 90 bar. The activated argon is injected in the detector trough a purifier (SAES MC1500-903) in a similar way as the standard argon. In order to reach the desired activity in the detector, a fixed volume of gas at known pressure was introduced several time. It is worth mentioning that a source based on ^{37}Ar also emits monoenergetic neutrinos of 811 keV, as considered for example in [10–12]. In the following, we will focus on demonstrating the usefulness of an ^{37}Ar source for low energy calibration of electromagnetic recoils in dual-phase detectors.

III. RESULTS

We report the results of our first measurements with ^{37}Ar. These measurements were taken with $E_{\rm drift} = 2.4$ kV/cm applied electric field across the active region, and 6.0 kV/cm across the 7 mm of liquid argon in the extraction region, which ensures $\sim$100% transmission of electrons from the liquid in to the gas phase [13]. The electric field in the gaseous amplification region was 9.0 kV/cm.

The waveform of each PMT was independently digitized and stored for off-line analysis. The trigger was set to acquire all four PMTs signals when two selected PMTs cross within 5 μs a given hardware threshold set just above the baseline noise. Each waveform is 100 μs long and includes a 35 μs pre-trigger.

The analysis of PMTs signals is performed following a gate-time algorithm similar to the one outlined in [14]. From each triggered waveform, the baseline is first com-
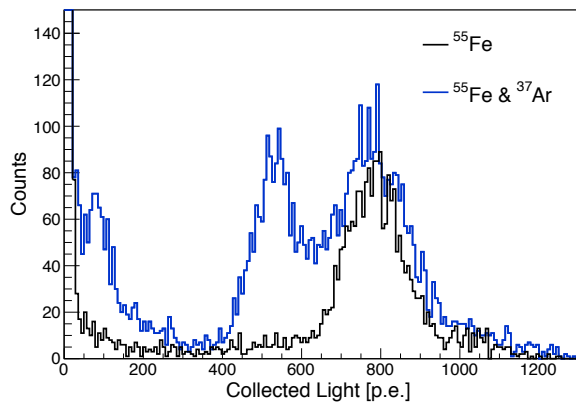
FIG. 2. Comparison of the spectra collected before (blue line) and after (black line) the injection of ^{37}Ar in the detector. The rightmost peak present in both spectra comes from the ^{55}Fe located inside the active volume. Data obtained with an electric field of 2.4 kV/cm in the drift region and of 9.0 kV/cm in the amplification region.

FIG. 3. Fit to the spectrum of the data collected after injection of ^{37}Ar. The peaks are due to the ^{55}Fe and ^{37}Ar calibration sources. The total fit is shown in black and the individual components of the fit as red dashed lines. Data obtained with an electric field of 2.4 kV/cm in the drift region and of 9.0 kV/cm in the amplification region. χ^2/d.o.f. = 125.5/115.

puted for each channel; software thresholds are then set based on the single photo-electron (s.p.e.) response of each PMT. All digitized points above threshold are grouped into a single event if their time gap is less than a given gate time across all 4 channels. A gate time of 3.5 μs is used for the analysis of the data reported here. Varying the gate time between 2 μs and 7.5 μs affects the results by $< 1\%$. The single photo-electron amplitude of each PMT is used to compute the total event energy in unit of s.p.e. across all channels.

The PMT's collection efficiency for secondary light varies by 30-40% for edge events with respect to central ones, simply because of geometry. In order to reduce this and other edge effects, a simple fiducialization algorithm was used to quantify the X-Y position of any event. For each of the four PMTs the number of detected p.e. is computed. The first fiducialization parameter is extracted from the ratio of the two PMTs on the east side vs the two PMTs on the west side; the second parameter from the north/south ratio. The ratios are taken so that the parameter is always greater than 1 and are then mapped to a square phase space of side 1. In the following a fiducialization cut that selects the central ∼40% of the active region volume is used.

Two additional basic cuts are used for event selection. First of all we require that the event start time is within 5 μs from the trigger position. We also request that no more than 3 s.p.e. are present in the pre-trigger and no more than 5 s.p.e. after the end of the event.

In Fig.2 we show the spectra collected before and after injecting ∼2 kBq of ^{37}Ar in our detector. Before injection, only the peak from the ^{55}Fe source is present. After the ^{37}Ar liquefied and mixed with the rest of the argon, two more peaks appeared from K- and L-shell electron capture of ^{37}Ar.

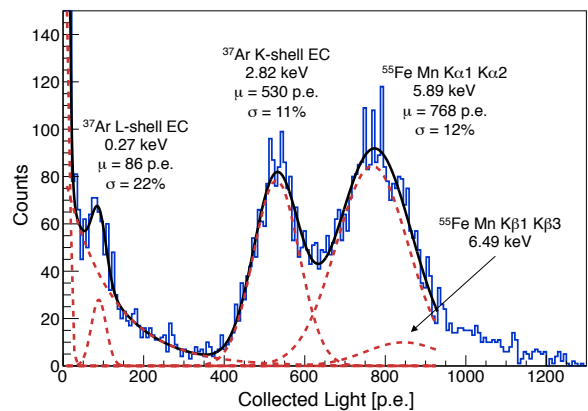The spectrum with ^{37}Ar is fitted in Fig.3. The low-

energy background is modeled with two exponentials. The ^{55}Fe source is described by two gaussians, one at 5.90 keV and the second at 6.49 keV. These values come from the weighted average of the four most prominent x-ray lines in the ^{55}Fe decay [15]. The relative amplitude of the two peaks was constrained accordingly to a factor (2.99/25.4). The width of the smaller peak at 6.49 keV was also fixed from the value of the primary 5.90 keV peak. The two ^{37}Ar peaks were also modeled with two independent gaussians.

A relative branching ratio of 0.116 ± 0.013 for the L- over K-shell EC for ^{37}Ar is calculated from the fit. This is in agreement with previous measurements in gaseous argon [16–19].

During the same run we were able to measure the detector response to single ionization electrons (i.e.). Single electron events appeared following electric discharge in the detector, their rate decreasing over the course of several hours. We are currently working to study and understand the production mechanism of this single electrons. Here we show in in Fig.4 the single electron spectrum. In order to study the population of single electrons, a stricter cut is applied, requiring less than 1 s.p.e. before or after each event. The fiducialization cut was removed as it is not effective at this very low number of p.e.. The average event width for single electrons was ∼6 μs, with longer events due to pile-up, as shown in the inset of Fig.4. The spectrum is fitted using two gaussians to describe single- and double-electrons events. The mean and width of the double-electrons gaussian are constrained from the values of the single electrons distribution. The single electron response is 8.2 p.e/i.e. with a 1 sigma resolution of 3.4 p.e..

Using the single electron response, we compute the number of electrons extracted from liquid argon for each
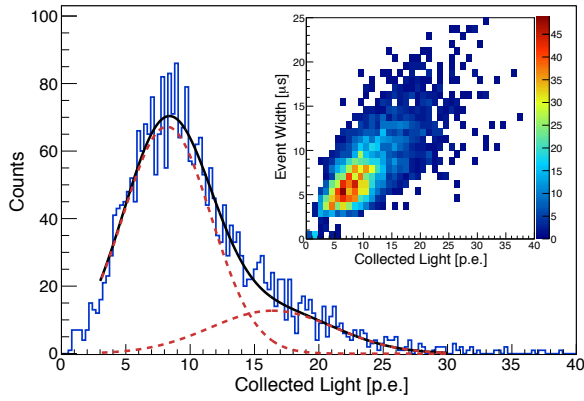
FIG. 4. Single electron spectrum obtained in the same electric field configuration of the [37]Ar data. The spectrum is fitted with two gaussians describing the single- and double-electrons events. Data obtained with an electric field of 2.4 kV/cm in the drift region and of 9.0 kV/cm in the amplification region. χ^2/d.o.f. = 115.4/94. In the inset, scatter plot of the event width vs the collected light in p.e. for the events in the spectrum.
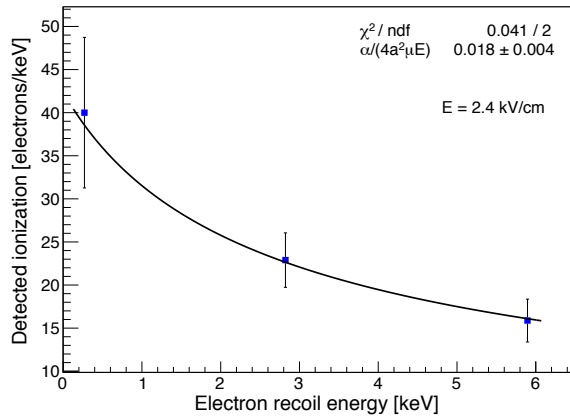

FIG. 5. Dependence of detected ionization in the [37]Ar and [55]Fe peaks from the spectrum of Fig.3 on the induced electron recoil energy. The solid curve is the result of the fit of the experimental data using the Thomas-Imel box model of eq. (1) and (2). The value of the single free fit parameter is provided in the figure. Data obtained at an electric field of 2.4 kV/cm.

of the three main peaks in Fig. 3. These are plotted in Fig. 5 as a function of the nominal energy deposited in the detector.

IV. DISCUSSION

It is interesting to compare the data in Fig. 5 against the Thomas–Imel box model [20] that predicts the fraction of electrons that escape recombination as

$$\frac{n_e}{N_i} = \frac{1}{\xi} \ln(1 + \xi), \quad \xi = \frac{N_i \alpha}{4a^2 uE} \qquad (1)$$

where α and u are the recombination and mobility coefficients, E the electric field and a the box dimension parameter. Following the suggestion in [4], the number of initial electrons N_i is calculated assuming a value $w_q = 19.5$ eV for the energy required to create a quanta (either ionization or excitation) in liquid argon [5] and an initial partitioning between the two channels of $N_{\mathrm{ex}}/N_i = 0.21$ [21]:

$$N_i = \frac{E_{er}}{w_q} \frac{1}{(1 + N_{\mathrm{ex}}/N_i)} \qquad (2)$$

Equation (1) is fitted to the data with $\alpha/(4a^2 uE)$ as a constant free parameter, as shown in Fig. 5. Excellent agreement of the model with experimental data suggests that it is applicable in liquid argon at low energies. An experimental verification of this behavior at different values of the drift electric field is currently being performed.

It is somewhat surprising that the data agrees with the model up to 6 keV. Previous work in liquid xenon [22] has shown that above a few keV electron recoil energy, recombination fluctuations begin to significantly modify the number of collected electrons. This is manifested as a departure from the Thomas-Imel prediction. Our data offers a preliminary suggestion that in liquid argon, recombination fluctuations are less significant in the few keV energy range.

In conclusion, we have shown that dual-phase argon ionization detectors are sensitive to sub-keV electron recoils. We have also provided a novel calibration technique in this energy range through the use of [37]Ar. This first demonstration of sensitivity in the sub-keV to few keV range in liquid argon enables the possibility of a sensitive search for axion-like particles, via the axio-electric effect [23]. We are also developing a technique to produce [37]Ar with no [39]Ar contamination. If this is successful, this calibration tool should be useful for liquid xenon detectors such as LUX [24]. Moreover, these data indicate that low-energy electron recoils in liquid argon can be modeled using a simple approach to electron recombination based on the Thomas–Imel box model. Efforts are underway to further corroborate these conclusions at different electric fields. We are also working to get experimental data on the ionization yield of low-energy nuclear recoils for the future development of both the CNNS and dark matter detectors.

---

[1] R. Gaitskell, Ann.Rev.Nucl.Part.Sci. **54**, 315 (2004).

[2] C. Hagmann and A. Bernstein, IEEE Trans. Nucl. Sci. **51**, 2151 (2004), arXiv:nucl-ex/0411004.

[3] J. Angle *et al.* (XENON10 Collaboration), Phys.Rev.Lett. **107**, 051301 (2011), arXiv:1104.3088 [astro-ph.CO].

[4] P. Sorensen and C. E. Dahl, Phys. Rev. **D83**, 063501 (2011), arXiv:1101.6080 [astro-ph.IM].

[5] T. Doke, A. Hitachi, J. Kikuchi, K. Masuda, H. Okada, and E. Shibamura, Japanese Journal of Applied Physics **41**, 1538 (2002).

[6] V. Chepel and H. Araujo, "Liquid noble gas detectors for low energy particle physics," (2012), arXiv:1207.2292 [physics.ins-det].

[7] S. Sangiorgio, A. Bernstein, J. Coleman, M. Foxe, C. Hagmann, T. Joshi, I. Jovanovic, K. Kazkaz, K. Movrokoridis, and S. Pereverzev, Physics Procedia **37**, 1266 (2012), proceedings of the 2nd International Conference on Technology and Instrumentation in Particle Physics (TIPP 2011).

[8] V. Boccone *et al.* (ArDM Collaboration), JINST **4**, P06001 (2009), arXiv:0904.0246 [physics.ins-det].

[9] C. Aalseth, A. Day, D. Haas, E. Hoppe, B. Hyronimus, *et al.*, Nucl.Instrum.Meth. **A652**, 58 (2011), arXiv:1008.0691 [nucl-ex].

[10] V. Barsanov, A. Dzhanelidze, S. Zlokazov, N. Kotelnikov, S. Y. Markov, *et al.*, Phys.Atom.Nucl. **70**, 300 (2007).

[11] J. Abdurashitov, V. Gavrin, S. Girin, V. Gorbachev, P. Gurkina, *et al.*, Phys.Rev. **C73**, 045805 (2006), arXiv:nucl-ex/0512041 [nucl-ex].

[12] J. A. Formaggio, E. Figueroa-Feliciano, and A. Anderson, Phys.Rev. **D85**, 013009 (2012), arXiv:1107.3512 [hep-ph].

[13] A. F. Borghesani, G. Carugno, M. Cavenago, and E. Conti, Physics Letters A **149**, 481484 (1990).

[14] K. Kazkaz, M. Foxe, A. Bernstein, C. Hagmann, I. Jovanovic, *et al.*, Nucl.Instrum.Meth. **A621**, 267 (2010), arXiv:0908.3277 [physics.ins-det].

[15] Chu, S.Y.F. and Ekström, L.P. and Firestone. R.B., "WWW table of radioactive isotopes, database version 2/28/1999," (1999).

[16] A. G. Santos-Ocampo and D. C. Conway, Phys. Rev. **120**, 2196 (1960).

[17] C. Manduchi and G. Zannoni, Il Nuovo Cimento **22**, 462 (1961).

[18] P. W. Dougan, K. W. D. Ledingham, and R. W. P. Drever, Philosophical Magazine **7**, 475 (1962).

[19] D. Totzek and K.-W. Hoffmann, Zeitschrift für Physik **205**, 137 (1967).

[20] J. Thomas and D. Imel, Phys.Rev. **A36**, 614 (1987).

[21] S. Kubota, A. Nakamoto, T. Takahashi, S. Konno, T. Hamada, M. Miyajima, A. Hitachi, E. Shibamura, and T. Doke, Physical Review B **13**, 1649 (1976).

[22] C. E. Dahl, *The physics of background discrimination in liquid xenon, and first results from Xenon10 in the hunt for WIMP dark matter*, Ph.D. thesis, Princeton University (2009).

[23] K. Arisaka, P. Beltrame, C. Ghag, J. Kaidi, K. Lung, *et al.*, "Expected Sensitivity to Galactic/Solar Axions and Bosonic Super-WIMPs based on the Axio-electric Effect in Liquid Xenon Dark Matter Detectors," (2012), arXiv:1209.3810 [astro-ph.CO].

[24] D. Akerib *et al.* (LUX Collaboration), "The Large Underground Xenon (LUX) Experiment," (2012), arXiv:1211.3788 [physics.ins-det].